URSI GASS 2023, Sapporo, Japan, 19-26 August 2023

Suppression of Mainlobe Deceptive Jammers with SF-RDA Radar

Lan Lan*(1), Guisheng Liao(1), Shengqi Zhu(1), Jingwei Xu(1), and Hing Cheung So(2)
(1) National Key Laboratory of Radar Signal Processing, Xidian University, Xi'an 710071, China; e-mail: lanlan@xidian.edu.cn; liaogs@xidian.edu.cn; zhushengqi8@163.com; xujingwei1987@163.com
(2) Department of Electrical Engineering, City University of Hong Kong, Kowloon, Hong Kong; e-mail: hcso@ee.cityu.edu.hk

Abstract

This paper addresses the problem of suppressing mainlobe deceptive jammers based on a novel stepped frequency (SF)-receive delay array (RDA) radar. In our system design, the linear frequency modulation waveform is transmitted with a SF across the transmit antenna elements, and the received echo is delayed with a time shift between adjacent receive elements. In this regard, the range-angle-dependent transmit and receive steering vectors are obtained, making it possible to distinguish the true target and the mainlobe deceptive jammers, especially those generated in the same transmit pulse behind the true target. Furthermore, a joint transmit-receive beamforming method is developed, including the data-independent transmit beamforming and the dimension-reduced data-dependent receive beamforming. Therefore, the jammers are suppressed by nulling in the joint transmit-receive spatial domain. Numerical simulations are provided to demonstrate the effectiveness of the proposed method in suppressing mainlobe deceptive jammers.

1 Introduction

Deceptive jammer is a common threat for radar systems, where multiple false targets are generated after modulation in the digital radio frequency memory (DRFM) [1]. More seriously, if the deceptive jammers are located in the mainlobe, beampattern distortion will occur. In order to address this issue, various approaches have been investigated in the frequency, time, spatial, and polarization domains [2–4]. Nevertheless, there are still considerable limitations in practice with traditional radar frameworks, such as the phased array and multiple-input multiple-output (MIMO). As a consequence, new frontiers have been opened for mainlobe deceptive jammer suppression, such as the frequency diverse array (FDA)-MIMO [5] and element-pulse coding (EPC)-MIMO radars [6].

Capitalizing a range-angle-dependent beampattern, the FDA-MIMO radar has received much attention in recent years [7]. By utilizing the extra degrees-of-freedom (DOFs) in the range domain, the mainlobe deceptive jammers are suppressed either due to range mismatch with the data-dependent beamforming or by nulling at the data-independent beampattern [5, 6]. However, suppression of the jammers, which lag behind the true target in the same transmit pulse, is not realizable with the aforementioned methods. Worse still, it is difficult to obtain ideal orthogonal waveforms within same frequency bandwidth for MIMO systems.

Following this guideline, the stepped frequency (SF)-receive delay array (RDA) radar is developed by transmitting a linear frequency modulation (LFM) waveform with a SF, and receiving the echo with a time delay between adjacent receive elements. In this respect, after appropriate processing procedures, the range-angle-dependent transmit and receive steering vectors can be obtained. Therefore, the true and false targets, especially those generated in the same transmit pulse behind the true target, can be discriminated in the joint transmit-receive spatial domain. Moreover, the false targets can be suppressed after performing the equivalent data-independent transmit beamforming and data-dependent receive beamforming. Numerical results are provided to verify the superiorities of the developed SF-RDA in jammer suppression, where a comparison among different radar frameworks is carried out in terms of the output power of matched filtering and output signal-to-interference-plus-noise ratio (SINR).

The paper is organized as follows. Section II presents the signal model of the SF-RDA radar. Principle of mainlobe deceptive jammer suppression with the joint transmit-receive beamforming is presented in Section III. Numerical examples are provided in Section IV, whereas conclusions are drawn in Section V.

Notations: The transpose and conjugate transpose operators are denoted by the symbols $(\cdot)^{\mathrm{T}}$ and $(\cdot)^{\dagger}$, respectively. $\mathbb{C}^N$, $\mathbb{R}^N$, and $\mathbb{C}^{N\times M}$ are respectively the sets of N-dimensional vectors of complex numbers, N-dimensional vectors of real numbers, and $N\times M$ complex matrices. $\odot$ and $\otimes$ represent the Hadamard (element-wise) product and Kronecker product, respectively. The letter j represents the imaginary unit (i.e. $j=\sqrt{-1}$). For any real number z, $|z|$ is used to denote the absolute value of z.

2 Signal Model of SF-RDA Radar

Let us consider a colocated MIMO radar system in a uniform linear array equipped with M transmit and N receive antenna elements with the first being the reference. Assuming that a SF LFM waveform is transmitted with a frequency interval Δf between two adjacent elements, and the transmitted signal is given as

$$x_m(t) = \sqrt{\frac{E}{M}}\varphi(t)\, e^{j2\pi f_m t}, 0 \le t \le T_p, \tag{1}$$

where E denotes the total transmitted energy, T_p is the radar pulse duration, $f_m = f_0 + (m-1)\Delta f$ indicates the m-th ($m = 1, \cdots, M$) SF with f_0 being the reference carrier frequency, and $\varphi(t) = e^{j\pi\mu t^2}/\sqrt{T_p}$ represents the LFM waveform with $\mu = B_w/T_p$ and B_w being the chirp rate and bandwidth, respectively. Notice that the orthogonality condition between adjacent transmit SF LFM waveforms is assumed to be satisfied.

Assuming a point-like target located in far-field with the angle-range pair (θ_0, R_0), and the target echo is received with a time delay $\Delta\tau$ across the receive elements, where the time delay corresponding to the n-th ($n = 1, \cdots, N$) receive antenna element is written as

$$t_n = (n-1)\Delta\tau. \tag{2}$$

Hence, under the narrowband assumption, the echo received by the n-th element, after multiplying by $e^{-j2\pi f_0 t}$, is expressed as

$$\begin{aligned}\bar{y}_n(t) \approx{}& \alpha_0\varphi(t-\tau_0)\, e^{-j2\pi\mu t_n t} e^{j2\pi\mu t_n\tau_0} e^{j\pi\mu t_n^2} \\ & e^{j2\pi\frac{(n-1)d\sin(\theta_0)}{\lambda_0}} e^{-j2\pi f_0 t_n} \sum_{m=1}^{M} e^{j2\pi\frac{(m-1)d\sin(\theta_0)}{\lambda_0}} \\ & e^{-j2\pi(m-1)\Delta f\tau_0} e^{j2\pi(m-1)\Delta f(t-t_n)},\end{aligned} \tag{3}$$

where $\tau_0 = 2R_0/c$ with c being the reference time delay, α_0 denotes the complex coefficient accounting for target backscattering and the other terms involved in the two-way radar equation, and the approximation holds by ignoring the terms $e^{j2\pi(m-1)^2\Delta f d\sin(\theta_0)/\lambda_0}$ and $e^{j2\pi(m-1)(n-1)\Delta f d\sin(\theta_0)/\lambda_0}$ due to the fact that $\Delta f d/c \ll 1$, and $\lambda_0 = c/f_0$.

Subsequently, the signal $\bar{y}_n(t)$ is processed with a multi-rate filter as

$$\begin{aligned}z_n(t) &= b_n(t_n)\,\bar{y}_n(t) \\ &= \alpha_0\varphi(t-\tau_0)\, e^{j2\pi\mu t_n\tau_0} e^{j2\pi\frac{(n-1)d\sin(\theta_0)}{\lambda_0}} \\ &\sum_{m=1}^{M} e^{j2\pi\frac{(m-1)d\sin(\theta_0)}{\lambda_0}} e^{-j2\pi(m-1)\Delta f\tau_0} e^{j2\pi(m-1)\Delta f(t-t_n)},\end{aligned} \tag{4}$$

where $b_n(t_n) = e^{j2\pi\mu t_n t} e^{-j\pi\mu t_n^2} e^{j2\pi f_0 t_n}$.

Then, it follows the procedure of processing with $f_{n,l}(t_n) = e^{-j2\pi(l-1)\Delta f(t-t_n)}$, namely

$$\begin{aligned}\bar{z}_{n,m}(t) &= f_{n,l}(t_n)\, z_n(t) = \alpha_0\varphi(t-\tau_0)\, e^{j2\pi\mu t_n\tau_0} \\ & e^{j2\pi\frac{(n-1)d\sin(\theta_0)}{\lambda_0}} e^{j2\pi\frac{(m-1)d\sin(\theta_0)}{\lambda_0}} e^{-j2\pi(m-1)\Delta f\tau_0}.\end{aligned} \tag{5}$$

Subsequently, processing through a bank of M waveform MFs, i.e., $h_l(t) = \varphi^*(-t)$, yields

$$\begin{aligned}\tilde{z}_{n,l} = \int_{-\infty}^{\infty} \bar{z}_{n,m}(t)(\tau) h_l(t-\tau)d\tau &= \alpha_0\mathrm{sinc}(\varphi)\, e^{j2\pi\mu t_n\tau_0} \\ e^{j2\pi\frac{(n-1)d\sin(\theta_0)}{\lambda_0}} e^{j2\pi\frac{(m-1)d\sin(\theta_0)}{\lambda_0}} & e^{-j2\pi(m-1)\Delta f\tau_0}.\end{aligned} \tag{6}$$

Therefore, the received signals from N receive elements can be stacked to form a MN-dimensional vector as

$$\begin{aligned}\boldsymbol{z}(\theta_0, R_0) &= [\tilde{z}_{1,1}, \tilde{z}_{1,2}, \cdots, \tilde{z}_{n,m}, \cdots \tilde{z}_{N,M}]^{\mathrm{T}} \\ &= \alpha_0\mathrm{sinc}(\varphi)\left[\boldsymbol{b}(\theta_0, R_0) \otimes \boldsymbol{a}(\theta_0, R_0)\right],\end{aligned} \tag{7}$$

where $\boldsymbol{b}(\theta_0, R_0) \in \mathbb{C}^N$ and $\boldsymbol{a}(\theta_0, R_0) \in \mathbb{C}^M$ denote the receive and transmit steering vectors of the target, respectively, with the forms of

$$\begin{aligned}\boldsymbol{b}(\theta_0, R_0) = \Bigg[1, \cdots, & e^{j2\pi\left(\frac{(n-1)d\sin(\theta_0)}{\lambda_0} + \mu\Delta\tau(n-1)\tau_0\right)}, \\ & \cdots, e^{j2\pi\left(\frac{(N-1)d\sin(\theta_0)}{\lambda_0} + \mu\Delta\tau(N-1)\tau_0\right)}\Bigg]^{\mathrm{T}},\end{aligned} \tag{8a}$$

$$\begin{aligned}\boldsymbol{a}(\theta_0, R_0) = \Bigg[1, \cdots, & e^{j2\pi\left(\frac{(m-1)d\sin(\theta_0)}{\lambda_0} - \Delta f(m-1)\tau_0\right)}, \\ & \cdots, e^{j2\pi\left(\frac{(M-1)d\sin(\theta_0)}{\lambda_0} - \Delta f(M-1)\tau_0\right)}\Bigg]^{\mathrm{T}}.\end{aligned} \tag{8b}$$

3 Principle of Mainlobe Deceptive Jammer Suppression with Joint Transmit-Receive Beamforming

Let us consider the type of self-defense jammers, where the false target generator (FTG) is equipped with the target, and Q false targets are generated after some appropriate modulations in DRFM. To this regard, the total received signal, including the true target, the false targets as well as the noise, is expressed as

$$\boldsymbol{w} = \boldsymbol{z}(\theta_0, R_0) + \sum_{q=1}^{Q} \boldsymbol{z}(\theta_q, R_q) + \boldsymbol{n}, \tag{9}$$

where $\boldsymbol{n} \in \mathbb{C}^{MN}$ is modelled as white Gaussian noise, $\boldsymbol{z}(\theta_q, R_q) \in \mathbb{C}^{MN}$ denotes the vector of the q-th ($q = 1, \cdots, Q$) false target, i.e.,

$$\boldsymbol{z}(\theta_q, R_q) = \mathrm{sinc}(\varphi)\,\alpha_q\left[\boldsymbol{b}(\theta_q, R_q) \otimes \boldsymbol{a}(\theta_q, R_q)\right], \tag{10}$$

where $\theta_q = \theta_0$, α_q is the complex echo amplitude, $\boldsymbol{b}(\theta_q, R_q) \in \mathbb{C}^N$ and $\boldsymbol{a}(\theta_q, R_q) \in \mathbb{C}^M$ represent the receive and transmit steering vectors with R_q being the actual range.

Particularly, as shown in Fig. 1, the false targets can be generated either in the same transmit pulse (i.e., the same range ambiguity region), such as the false target 1, or in the next transmit pulse, such as the false targets 2 and 3. More specifically, in the same range ambiguity region, the false target can be behind (such as the false targets 1 and 3) or settled ahead of the true target (such as the false target 2).

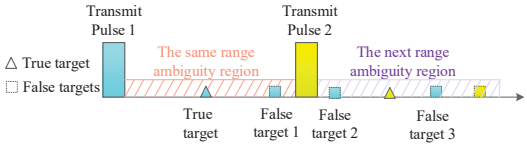

Figure 1. Generation of false targets.

Furthermore, a compensation procedure is performed range-by-range on the transmit steering vectors [5], which yields the normalized receive spatial frequencies as

$$f_{\mathrm{T}}^{\mathrm{s}} = -\frac{2\Delta f}{c} p_s R_u + \frac{d}{\lambda_0}\sin(\theta_0), \tag{11a}$$

$$f_{\mathrm{T}}^{q} = -\frac{2\Delta f}{c} p_q R_u + \frac{d}{\lambda_0}\sin(\theta_0), \tag{11b}$$

where p_s and p_q denote the numbers of delayed transmit pulses corresponding to the true and q-th false target, respectively, R_u indicates the maximum unambiguous range. Furthermore, the receive spatial frequencies of the true target and the q-th false target are respectively defined as

$$f_{\mathrm{R}}^{\mathrm{s}} = \mu\Delta\tau\frac{2R_0}{c} + \frac{d}{\lambda_0}\sin(\theta_0), \tag{12a}$$

$$f_{\mathrm{R}}^{q} = \mu\Delta\tau\frac{2R_q}{c} + \frac{d}{\lambda_0}\sin(\theta_0), \tag{12b}$$

indicating that the true and false targets can be discriminated in both transmit and receive spatial frequencies.

To proceed, a joint transmit-receive beamforming method is implemented, where an equivalent data-independent transmit beamforming is firstly implemented in each receive channel, with the transmit weight vector obtained as $\boldsymbol{w}_{\mathrm{T}} = \boldsymbol{a}(\theta_0, R_0) \in \mathbb{C}^M$. In this respect, the jammers, which are located in different range ambiguity regions compared with the true one, can be suppressed by nulling at the equivalent transmit beampattern, Accordingly, the frequency interval can be designed as

$$\Delta f = f_r\left(\ell + \frac{i}{(p_q - p_s)M}\right), \tag{13}$$

where $\ell = \mathrm{int}(\Delta f / f_r)$ denotes the integer part.

Moreover, the dimension of the received echo is reduced as

$$\tilde{\boldsymbol{y}} = \boldsymbol{W}_{\mathrm{re}}\hat{\boldsymbol{y}}, \tag{14}$$

where $\tilde{\boldsymbol{y}} \in \mathbb{C}^N$, $\hat{\boldsymbol{y}} \in \mathbb{C}^{MN}$, and $\boldsymbol{W}_{\mathrm{re}} = \mathrm{diag}\left\{\boldsymbol{w}_{\mathrm{T}}^{\dagger}, \cdots, \boldsymbol{w}_{\mathrm{T}}^{\dagger}\right\} \in \mathbb{C}^{N\times MN}$ denotes the dimension-reduced matrix.

Furthermore, the data-dependent beamforming is performed based on the minimum variance distortionless response (MVDR) criterion by solving the following optimization problem

$$\begin{cases} \min\limits_{\boldsymbol{w}_{\mathrm{R}}} & \boldsymbol{w}_{\mathrm{R}}^{\dagger}\boldsymbol{R}\boldsymbol{w}_{\mathrm{R}} \\ \text{s.t.} & \boldsymbol{w}_{\mathrm{R}}^{\dagger}\boldsymbol{b}(\theta_0, R_0) = 1 \end{cases}, \tag{15}$$

where $\boldsymbol{R} \in \mathbb{C}^{N\times N}$ is the jammer-pulse-noise covariance matrix, which is obtained with $\tilde{\boldsymbol{y}}$, and the receive weight vector is obtained as $\boldsymbol{w}_{\mathrm{R}} = \boldsymbol{R}^{-1}\boldsymbol{b}(\theta_0, R_0)$. In this regard, the false targets which are located in the same range ambiguity region, are suppressed due to range mismatch. Finally, by combining both the transmit and receive weight vectors, the weight vector in the joint transmit-receive spatial domain is determined as:

$$\boldsymbol{w}_{\mathrm{o}} = \boldsymbol{w}_{\mathrm{R}} \otimes \boldsymbol{w}_{\mathrm{T}}. \tag{16}$$

4 Simulation Results

In this section, numerical examples are provided to assess the effectiveness of jammer suppression with the SF-RDA radar. The system parameters are listed in Table I, whereas parameters of the true and $Q = 4$ false targets are presented in Table II.

Table 1. System parameters of RDA

Parameter	Value	Parameter	Value
M	10	N	16
f_0	10 GHz	Δf	10.006 MHz
B_w	10 MHz	PRF	10 KHz
T_p	10 μs	$\Delta\tau$	100 ns
R_u	15 km	L	1000

Table 2. Parameters of true and false targets

	True	False 1	False 2	False 3	False 4
Angle (°)	0	0	0	0	0
Range (km)	3	4	6.7	27	31.5
Delay pulses	0	0	0	1	2
SNR/JNR (dB)	15	35	35	35	35
Range bin	201	268	448	801	101

The Capon spectrum of the true and false targets in the joint transmit-receive spatial frequency domain is displayed in Fig. 2(a), where all targets are distributed in both the transmit and receive spastical frequencies. Correspondingly, the two-dimensional beampattern is shown in Fig. 2(b). It is observed that the maximum is achieved in the position of the true target, while the false targets are located at the nulls. Moreover, performance comparisons in terms of the matched filtering and output SINR are carried out among the developed SF-RDA, conventional MIMO, FDA-MIMO, as well as EPC-MIMO in Figs. 2(c) and (d). Figures inspections indicate that all false targets are unavailable to be suppressed in MIMO radar due to lack of DOFs

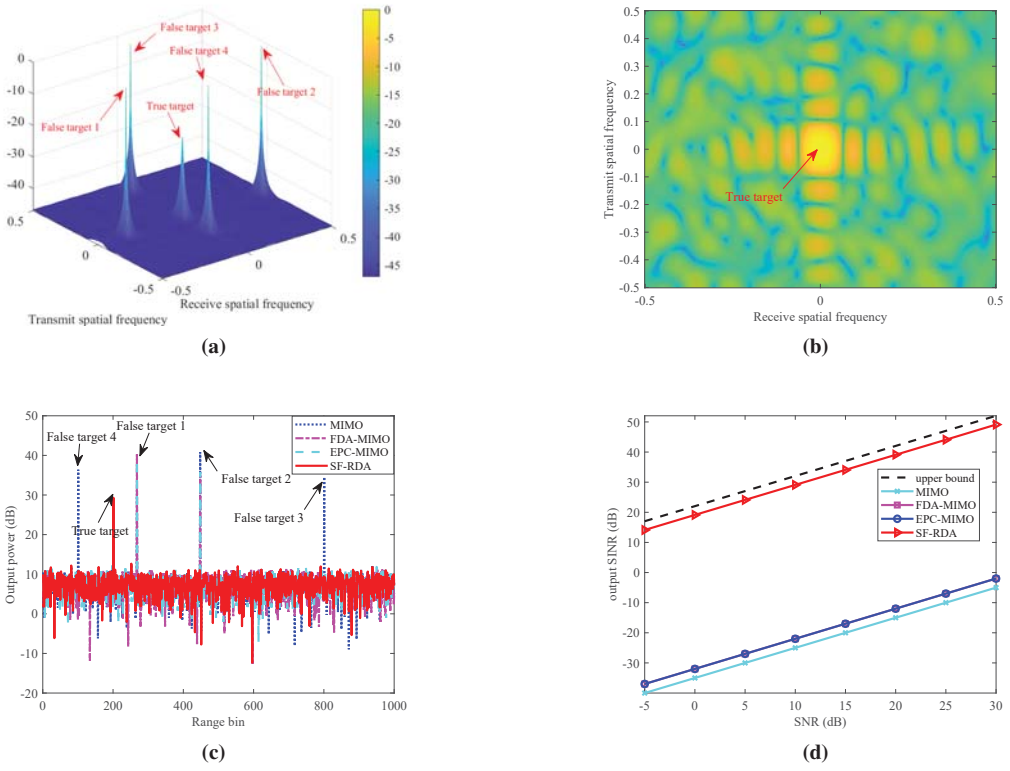

Figure 2. Jammer suppression with SF-RDA radar. (a) Capon spectrum. (b) Beampattern. (c) Matched filtering. (d) Output SINR.

in the range domain. In addition, the false targets 3 and 4, which are located in different range ambiguity regions of the true one, can be suppressed with both the FDA-MIMO and EPC-MIMO. However, they cannot suppress the false targets 1 and 2, which are located in the same range ambiguity region with the true one. In contrast, all false targets are sufficiently suppressed with the proposed SF-RDA radar, with a SINR improvement over 50 dB compared with that of the MIMO radar, corroborating the advantages of D-OFs in the joint transmit receive spatial frequency domain offered by the SF-RDA radar.

5 Conclusions

In this paper, the SF-RDA radar has been developed by transmitting the LFM waveform with a SF between transmit elements and receiving the echoes with a time shift across the receive elements. After appropriate receive processing, the true and false targets can be distinguished in the joint transmit-receive spatial domain. Moreover, a joint transmit-receive beamforming method has been implemented to suppress the false targets. Simulations in terms of output matched filtering and SINR have been carried out to verify the effectiveness of jammer suppression, especially for those located in the same range ambiguity region with the true target, where significant SINR improvements compared with the MIMO, FDA-MIMO and EPC-MIMO have been illustrated. Possible future research avenues might be focused on the extension to a scenario including clutter.

References

[1] A. Gupta and V. Krishnamurthy, "Principal agent problem as a principled approach to electronic counter-countermeasures in radar," *IEEE Trans. Aerosp. Electron. Syst.*, vol. 58, no. 4, pp. 3223-3235, Feb. 2022.

[2] X. Zhang, D. Cao, and L. Xu, "Joint polarisation and frequency diversity for deceptive jamming suppression in MIMO radar," *IET Radar Sonar Navig.*, vol. 13, no. 2, pp. 263-271, Feb. 2019.

[3] J. Akhtar, "Orthogonal block coded ECCM schemes against repeat radar jammers," *IEEE Trans. Aerosp. Electron. Syst.*, vol. 45, no. 3, pp. 1218-1226, July 2009.

[4] X. Yang, Z. Zhang, T. Zeng, T. Long and T. K. Sarkar, "Mainlobe interference suppression based on eigen-projection processing and covariance matrix reconstruction," *IEEE Ant. Wireless Propag. Lett.,* vol. 13, pp. 1369-1372, Jul. 2014.

[5] L. Lan, J. Xu, G. Liao, Y. Zhang, F. Fioranelli, and H. C. So, "Suppression of mainbeam deceptive jammer with FDA-MIMO radar," *IEEE Trans. Vehi. Techn.*, vol. 69, no. 10, pp. 11584-11598, Oct. 2020.

[6] L. Lan, G. Liao, J. Xu, Y. Zhang, and S. Zhu, "Mainlobe deceptive jammer suppression with element-pulse coding MIMO radar," *Signal Process.*, vol. 182, pp. 1-14, Dec. 2020.

[7] J. Xu, G. Liao, S. Zhu, L. Huang, and H.-C. So, "Joint range and angle estimation using MIMO radar with frequency diverse array," *IEEE Trans. Signal Process.*, vol. 63, no. 13, pp. 3396-3410, Jul. 2015.